

Testing physical models for dipolar asymmetry with CMB polarization

D. Contreras,^{1,*} J. P. Zibin,^{1,†} D. Scott,^{1,‡} A. J. Banday,^{2,3,§} and K. M. Górski^{4,5,¶}

¹*Department of Physics & Astronomy
University of British Columbia, Vancouver, BC, V6T 1Z1 Canada*

²*Université de Toulouse
UPS-OMP, IRAP, F-31028 Toulouse cedex 4, France*

³*CNRS, IRAP
9 Av. colonel Roche, BP 44346, F-31-28 Toulouse cedex 4, France*

⁴*Jet Propulsion Laboratory, California Institute of Technology
4800 Oak Grove Drive, Pasadena, California, U.S.A*

⁵*Warsaw University Observatory
Aleje Ujazdowskie 4, 00-478 Warszawa, Poland
(Dated: April 12, 2017)*

The cosmic microwave background (CMB) temperature anisotropies exhibit a large-scale dipolar power asymmetry. To determine whether this is due to a real, physical modulation or is simply a large statistical fluctuation requires the measurement of new modes. Here we forecast how well CMB polarization data from *Planck* and future experiments will be able to confirm or constrain physical models for modulation. Fitting several such models to the *Planck* temperature data allows us to provide predictions for polarization asymmetry. While for some models and parameters *Planck* polarization will decrease error bars on the modulation amplitude by only a small percentage, we show, importantly, that cosmic-variance-limited (and in some cases even *Planck*) polarization data can decrease the errors by considerably better than the expectation of $\sqrt{2}$ based on simple ℓ -space arguments. We project that if the primordial fluctuations are truly modulated (with parameters as indicated by *Planck* temperature data) then *Planck* will be able to make a 2σ detection of the modulation model with 20–75% probability, increasing to 45–99% when cosmic-variance-limited polarization is considered. We stress that these results are quite model dependent. Cosmic variance in temperature is important: combining statistically isotropic polarization with temperature data will spuriously increase the significance of the temperature signal with 30% probability for *Planck*.

PACS numbers:

I. INTRODUCTION

The largest scales of our cosmic microwave background (CMB) temperature sky exhibit a dipolar asymmetry with an amplitude at the percent level [1–5]. While the cosmological origin of this signal is not in dispute (existing in both WMAP and *Planck* data with very different systematic effects and frequency coverage), its statistical significance is debated (see [3, 5] and references therein). Without correction for the effects of a *a posteriori* selection, this large-scale signal has a significance at approximately the 3σ level, and an amplitude of roughly 6–7%, when restricted to a multipole range of $\ell \lesssim 65$. Applying look-elsewhere correction on the maximum multipole reduces the corresponding p -value to of order 10% [3, 5]. However, the asymmetry is present on scales that are roughly super-Hubble at last scattering, suggesting a possible physical origin related to very-early-Universe physics. If this were the case, the former significance estimate might be more relevant given a model that predicted it.

The dipolar asymmetry in temperature is now characterized as well as it ever will be, because the measurements on these scales are limited by cosmic variance and hence essentially all the cosmological information has already been extracted. The only way to determine if this signal is due to a physical modulation of fluctuations or is just a statistical fluke is to acquire new information (i.e., measure new and independent modes [6]). This can be achieved with the addition of large-scale polarization data. Polarization data are available from the *Planck* satellite; however, residual systematics (particularly at large angular scales) have so far prevented a full investigation of the polarization dipole asymmetry signal. Other probes of new modes that have been examined in this context include large-scale structure [7–10], CMB lensing [11, 12], and 21 cm measurements [13].

The use of polarization in the investigation of dipole asymmetry has been examined previously in Refs. [14–23]. In particular, it was appreciated [14, 22] that a modulation model must be constructed in position (or k) space and propagated to map (or spherical harmonic) space in order to consistently describe both temperature and polarization modes. In addition, it was found that the predicted signature in polarization is quite dependent on the assumed model for the k -space modulation [22]. Here we will use the temperature data to predict the polarization signature given a k -space modulation model, following the formalism developed in

*Electronic address: dagocont@phas.ubc.ca

†Electronic address: zibin@phas.ubc.ca

‡Electronic address: dscott@phas.ubc.ca

§Electronic address: anthony.banday@irap.omp.eu

¶Electronic address: krzysztof.m.gorski@jpl.nasa.gov

Ref. [11].

Naively, one might expect that the temperature signal, together with the assumption of a physical modulation of the large-scale three-dimensional fluctuation field, would predict a roughly 6–7% asymmetry in polarization in the ℓ range of 2 to 65. However, this is not necessarily the case, since the mapping (transfer functions) from k to ℓ space differs between temperature and polarization. Therefore, in the absence of a detailed physical modulation model we cannot use polarization to test for such a physical origin. In addition, as stressed in Ref. [11], the signal in the temperature data alone is not strong enough to pick out a well-defined modulation in k space. In this paper we will explore how these issues are modified with the inclusion of polarization data in more detail.

One well-known concern when considering polarization is the correlation between temperature and gradient- (or E -) mode polarization. More specifically, modes we can measure from polarization are not completely independent of temperature. This correlation may alter a possible polarization asymmetry signal or mimic such a signal in its absence. We deal with the correlation by calibrating our estimator on *Planck* Full Focal Plane (FFP8) temperature and polarization simulations [24] that are appropriately correlated. A further concern is the spurious enhancement of a modulation signal when including polarization. That is, simply due to cosmic variance and noise, adding polarization to temperature might sometimes increase the significance of a signal even when there is no true underlying modulation. This is especially true when the original temperature signal is of low to moderate significance, as is the case with our real CMB sky. We address this concern by quantifying the expected effect of adding polarization both with and without an underlying physical modulation.

Our main goals here are to determine how likely it is that a physical origin for a modulation could be confirmed, and to quantify the expected improvement in constraints on the k -space modulation model parameters, with the addition of polarization data. We will present projections for *Planck* as well as a cosmic-variance-limited polarization measurement. We will *not* perform a blind multipole-space dipole asymmetry search as has been done with temperature, though this can be done with the estimator we employ here and will be important to perform once the data are available.

For this study we use the FFP8 cosmological parameters, with Hubble parameter $H_0 = 100h \text{ km s}^{-1} \text{ Mpc}^{-1}$, where $h = 0.6712$, baryon density $\Omega_b h^2 = 0.0222$, cold dark matter (CDM) density $\Omega_c h^2 = 0.1203$, neutrino density $\Omega_\nu h^2 = 0.00064$, cosmological constant density parameter $\Omega_\Lambda = 0.6823$, primordial comoving curvature perturbation power spectrum amplitude $A_s = 2.09 \times 10^{-9}$ (at pivot scale $k_0 = 0.05 \text{ Mpc}^{-1}$) and tilt $n_s = 0.96$, and optical depth to reionization $\tau = 0.065$.

Note that at high ℓ our results would be biased due to the effect of aberration [25], which is not present in the FFP8 simulations [24]. In Appendix C we describe how we detect aberration in the temperature data and

remove it so as not to bias our results.

II. MODULATION APPROACH

A. Formalism

Our goal is to construct position- or k -space models that generate scale-dependent dipolar asymmetry, while remaining agnostic as to the detailed origin (presumably inflationary) of the modulation. Based on the temperature signal, we would like to modulate the largest scales while maintaining consistency with the usual isotropic Λ CDM power spectra. We consider three different types of model: the first is a modulated adiabatic mode which comprises a part of the total primordial power spectrum [45]; the second is a modulated CDM isocurvature mode; and the third is a modulated tensor mode. For the adiabatic scalar case, we must modulate a large-scale part of the spectrum. The contributions from CDM isocurvature and tensor modes, however, are naturally restricted to scales $\ell \lesssim 100$ (at least for near-scale-invariant spectra). Therefore in these cases we only need to apply a scale-invariant modulation to the tensor or isocurvature component. We will analyze each of these models with a slight generalization of the approach in [11], which considered only the adiabatic scalar case, and we refer to that reference for full details. Our approach will be readily applicable to other modulation models.

We begin by decomposing the primordial fluctuations into two components. The first, $\tilde{Q}^{\text{lo}}(\mathbf{x})$, is dipole modulated, i.e., spatially linearly modulated, and takes the form

$$\tilde{Q}^{\text{lo}}(\mathbf{x}) = Q^{\text{lo}}(\mathbf{x}) \left(1 + A \frac{\mathbf{x} \cdot \hat{\mathbf{d}}}{r_{\text{LS}}} \right), \quad (1)$$

where $Q^{\text{lo}}(\mathbf{x})$ is statistically isotropic with power spectrum $\mathcal{P}^{\text{lo}}(k)$, A is the modulation amplitude, $\hat{\mathbf{d}}$ is the direction of modulation, and r_{LS} is the comoving distance to last scattering. The second, unmodulated component, $Q^{\text{hi}}(\mathbf{x})$, is statistically isotropic with power spectrum $\mathcal{P}^{\text{hi}}(k)$. The two fields are uncorrelated, i.e.,

$$\langle Q^{\text{lo}}(\mathbf{k}) Q^{\text{hi}*}(\mathbf{k}') \rangle = 0. \quad (2)$$

The field $\tilde{Q}^{\text{lo}}(\mathbf{x})$ will correspond to the isocurvature, tensor, or modulated adiabatic component, while $Q^{\text{hi}}(\mathbf{x})$ will be the remaining, unmodulated adiabatic component. The superscripts “lo” and “hi” refer to the fact that generally these components will dominate at low and high k , respectively. Strictly we should consider only amplitudes $A \leq 1$, since for larger A the fluctuations in Eq. (1) will vanish somewhere inside the last scattering surface and the details in this case may depend on the specific (inflationary) realization of the model.

As shown in Ref. [11], the total temperature anisotropies will be given to very good approximation

by the sum of the uncorrelated contributions from the modulated and unmodulated fluctuations, i.e.,

$$\frac{\delta T(\hat{\mathbf{n}})}{T_0} = \frac{\delta T^{\text{lo}}(\hat{\mathbf{n}})}{T_0} (1 + A \hat{\mathbf{n}} \cdot \hat{\mathbf{d}}) + \frac{\delta T^{\text{hi}}(\hat{\mathbf{n}})}{T_0}. \quad (3)$$

The anisotropies $\delta T^{\text{lo}}/T_0$, with power spectrum $C_\ell^{T,\text{lo}}$, are generated by the perturbations with power spectrum $\mathcal{P}^{\text{lo}}(k)$, while $\delta T^{\text{hi}}/T_0$, with spectrum $C_\ell^{T,\text{hi}}$, are generated by the uncorrelated perturbations with power spectrum $\mathcal{P}^{\text{hi}}(k)$. The form of Eq. (3) is easy to understand in the limit where the anisotropies are much smaller than the length scale of modulation (i.e., r_{LS}). The large-scale case is less obvious, but Eq. (3) still holds to very good approximation [11]. Similarly, we have for the E -mode polarization anisotropies

$$\frac{\delta E(\hat{\mathbf{n}})}{T_0} = \frac{\delta E^{\text{lo}}(\hat{\mathbf{n}})}{T_0} (1 + A \hat{\mathbf{n}} \cdot \hat{\mathbf{d}}) + \frac{\delta E^{\text{hi}}(\hat{\mathbf{n}})}{T_0}. \quad (4)$$

In terms of spherical harmonic coefficients, the total fluctuations in Eq. (3) can be written as

$$a_{\ell m} = a_{\ell m}^{\text{lo}} + a_{\ell m}^{\text{hi}} + \sum_M \Delta X_M \sum_{\ell' m'} a_{\ell' m'}^{\text{lo}} \xi_{\ell m \ell' m'}^M, \quad (5)$$

where $a_{\ell m}^{\text{lo}}$ are the statistically isotropic modes, and the ΔX_M are the spherical harmonic decomposition of $A \hat{\mathbf{n}} \cdot \hat{\mathbf{d}}$ (the dipolar nature ensures that $M = -1, 0, 1$). The $\xi_{\ell m \ell' m'}^M$ are coupling coefficients given by

$$\xi_{\ell m \ell' m'}^0 = \delta_{m' m} (\delta_{\ell' \ell-1} A_{\ell-1 m} + \delta_{\ell' \ell+1} A_{\ell m}), \quad (6)$$

$$\xi_{\ell m \ell' m'}^{\pm 1} = \delta_{m' m \mp 1} (\delta_{\ell' \ell-1} B_{\ell-1 \pm m-1} - \delta_{\ell' \ell+1} B_{\ell \mp m}), \quad (7)$$

where

$$A_{\ell m} = \sqrt{\frac{(\ell+1)^2 - m^2}{(2\ell+1)(2\ell+3)}}, \quad (8)$$

$$B_{\ell m} = \sqrt{\frac{(\ell+m+1)(\ell+m+2)}{2(2\ell+1)(2\ell+3)}}. \quad (9)$$

From Eq. (5) we can find the covariance of the total temperature or polarization anisotropy multipoles to first order in the modulation amplitude $\Delta X \equiv \sqrt{\sum_M |\Delta X_M|^2} = A$:

$$C_{\ell m \ell' m'} \equiv \langle a_{\ell m} a_{\ell' m'}^* \rangle \quad (10)$$

$$= C_\ell \delta_{\ell \ell'} \delta_{m m'} + \frac{\delta C_{\ell \ell'}}{2} \sum_M \Delta X_M \xi_{\ell m \ell' m'}^M, \quad (11)$$

where $\delta C_{\ell \ell'} \equiv 2(C_\ell^{\text{lo}} + C_{\ell'}^{\text{lo}})$. The above equation explicitly shows that a dipole modulation will lead to coupling of ℓ to $\ell \pm 1$ modes in the multipole covariance [26]. In Eq. (11) C_ℓ is the total isotropic power spectrum, which, since the two fluctuation components are uncorrelated, is given to linear order in the asymmetry by

$$C_\ell^T = C_\ell^{T,\text{lo}} + C_\ell^{T,\text{hi}}, \quad (12)$$

and similarly for polarization. Clearly C_ℓ^T must be consistent with measurements of the isotropic power. For the adiabatic cases, we take

$$\mathcal{P}_\mathcal{R}^{\text{lo}}(k) + \mathcal{P}_\mathcal{R}^{\text{hi}}(k) = \mathcal{P}_\mathcal{R}^{\Lambda\text{CDM}}(k), \quad (13)$$

where

$$\mathcal{P}_\mathcal{R}^{\Lambda\text{CDM}}(k) = A_s \left(\frac{k}{k_0} \right)^{n_s-1} \quad (14)$$

is the comoving curvature power spectrum for ΛCDM , so that the isotropic power constraints are automatically satisfied. However, constraints on isocurvature and tensor contributions [27–29] should be incorporated [30] in addition to the constraints from the temperature asymmetry in order to obtain the tightest constraints for those models.

B. Adiabatic modulation

1. tanh spectrum

For scalar adiabatic modes [11] the fluctuation fields $Q^{\text{lo}}(\mathbf{x})$ and $Q^{\text{hi}}(\mathbf{x})$ both correspond to the comoving curvature perturbation, \mathcal{R} . Our first specific model is intended to capture a large-scale modulation with a small number of parameters. We choose a modulated component spectrum of the form

$$\mathcal{P}_\mathcal{R}^{\text{lo}}(k) = \frac{1}{2} \mathcal{P}_\mathcal{R}^{\Lambda\text{CDM}}(k) \left[1 - \tanh \left(\frac{\ln k - \ln k_c}{\Delta \ln k} \right) \right]. \quad (15)$$

This smooth step function in k ensures that mainly the largest scales ($k \lesssim k_c$) are modulated. The quantity $\Delta \ln k$ defines the sharpness of the transition from modulated to unmodulated scales. The other parameters of the model are the amplitude of modulation ($A = A_\mathcal{R}$) and its direction (l, b) in Galactic coordinates. The unmodulated contribution is fixed by Eq. (13). It must be noted that the temperature data alone are not strong enough to constrain all five modulation parameters ($k_c, \Delta \ln k, A_\mathcal{R}, l, b$); see Ref. [11]. The shapes of the best-fit asymmetry spectra for the tanh model (and all of the others) will be illustrated in Sec. IV A.

As shown in detail in [11], the fact that we have split the adiabatic fluctuations into two uncorrelated parts does not restrict the modulation mechanism (presumably inflationary) in any way. Instead this is a convenient way to describe an adiabatic spectrum modulated with arbitrary scale dependence.

2. Power-law spectrum

The tanh modulation model in Eq. (15) is not explicitly motivated by any early-Universe model. Perhaps

better motivated would be a simple power-law modulation, i.e.,

$$\mathcal{P}_{\mathcal{R}}^{\text{lo}}(k) = \mathcal{P}_{\mathcal{R}}^{\Lambda\text{CDM}}(k_0^{\text{lo}}) \left(\frac{k}{k_0^{\text{lo}}} \right)^{n_s^{\text{lo}} - 1}, \quad (16)$$

where n_s^{lo} is the tilt and k_0^{lo} is the pivot scale of the modulated component of fluctuations. This model will be abbreviated “ad.-PL”. We again impose Eq. (13) in order to define the unmodulated $\mathcal{P}_{\mathcal{R}}^{\text{hi}}(k)$. We consider only red tilts with $n_s^{\text{lo}} \leq n_s$, and choose $k_0^{\text{lo}} = 1.5 \times 10^{-4} \text{ Mpc}^{-1}$, which corresponds roughly to quadrupolar angular scales. Larger k_0^{lo} would contradict the positivity of $\mathcal{P}_{\mathcal{R}}^{\text{hi}}(k)$ on the largest observable scales, while smaller k_0^{lo} would be degenerate with the modulation amplitude. Again we modulate $\mathcal{P}_{\mathcal{R}}^{\text{lo}}(k)$ with amplitude $A_{\mathcal{R}}$, so the total modulation fraction approaches $A_{\mathcal{R}}$ on large angular scales. This model also should be taken with some caution, since for large departures from scale invariance (i.e., $1 - n_s^{\text{lo}} \not\ll 1$), we might expect higher-order terms such as running and running of running, etc. in the modulation spectrum.

3. Modulated scalar spectral index

Next we consider a single-component adiabatic model with a linear gradient in the tilt, n_s , of the primordial power spectrum. We abbreviate this model “ n_s -grad”. In this case we do not strictly follow the two-component formalism of Sec. II A, but instead can directly write the asymmetry spectrum as [31]

$$C_{\ell}^{\text{lo}} = -\frac{1}{2} \frac{dC_{\ell}^{\Lambda\text{CDM}}}{dn_s}. \quad (17)$$

Here we have used a linear approximation for the effect of the gradient, which will be well justified by our results. We allow for free modulation amplitude, Δn_s , and let the tilt pivot scale, k_* , vary. Note that this treatment is degenerate with fixed pivot k_* and additional modulation of the primordial amplitude, A_s . Since a modulation of tilt produces extra power on large scales in the $-\hat{\mathbf{d}}$ direction, we have included a minus sign in Eq. (17) so that the best-fit modulation directions will be directly comparable to those of the other models.

C. Tensor modulation

The possibility that a modulated tensor component is present is particularly well motivated observationally [32, 33], since the contribution of (near-scale-invariant or red-tilted) tensors is negligible at small scales. Tight constraints on the tensor-to-scalar ratio r will make it difficult to achieve sufficient modulation, however, via the isotropic power constraint [30].

In this case we take the unmodulated component $Q^{\text{hi}}(\mathbf{x})$ to be adiabatic fluctuations with the standard ΛCDM form, Eq. (14). The modulated component

$Q^{\text{lo}}(\mathbf{x})$ will be a scale-invariant tensor contribution with $r_{0.05} = 0.07$ (this is the 95% upper limit from [29]), i.e.,

$$\mathcal{P}_t(k) = r_{0.05} \mathcal{P}_{\mathcal{R}}^{\Lambda\text{CDM}}(k_0), \quad (18)$$

where we have used the pivot scale $k_0 = 0.05 \text{ Mpc}^{-1}$. The tensor modes are uncorrelated with the adiabatic fluctuations (note that even in the presence of such correlations, the scalar and tensor anisotropy power spectra would still be additive [34]) and modulated in a *scale-invariant* way with amplitude $A = A_t$. As before, the tensors produce anisotropy power $C_{\ell}^{T,\text{lo}}$ (and similarly for E).

D. Isocurvature modulation

Also well motivated as a modulation model is the CDM isocurvature spectrum, since it naturally contributes mainly at large angular scales for near-scale-invariant (or red-tilted) isocurvature modes. In this case we assume that the unmodulated $Q^{\text{hi}}(\mathbf{x})$ is an adiabatic contribution which takes the standard, ΛCDM form, Eq. (14). The modulated part $Q^{\text{lo}}(\mathbf{x})$ will be the isocurvature component, which we take to be scale-invariant, i.e.,

$$\mathcal{P}_{\mathcal{I}}(k) = \frac{\alpha}{1 - \alpha} \mathcal{P}_{\mathcal{R}}^{\Lambda\text{CDM}}(k_0), \quad (19)$$

where we use the same pivot scale k_0 as for the tensors. The isocurvature modes are taken to be uncorrelated with the adiabatic fluctuations and modulated in a *scale-invariant* way with amplitude $A = A_{\mathcal{I}}$. This isocurvature spectrum then determines the modulated component of the CMB fluctuations, C_{ℓ}^{lo} . The isocurvature fraction, α , should properly be constrained by the isotropic *Planck* likelihood [30], but here we simply choose the *Planck* upper limit for uncorrelated, *scale-invariant* isocurvature, $\alpha = 0.04$ [27].

III. DIPOLE ASYMMETRY ESTIMATOR

In this section we describe the estimator that we use to extract modulation parameters from data or simulations given a modulation model. This estimator is applied in harmonic space, exploiting the fact that (to leading order in the anisotropy) dipole modulation is equivalent to the coupling of ℓ with $\ell \pm 1$ modes, as we saw in Sec. II A.

A. Connection to previous approaches

The estimator that we use was originally developed for temperature data [5, 11, 31], but can equally be applied to polarization. Our current implementation includes new improvements to the treatment compared with [5, 11] in order to account for the expectation of noisy polarization data. Differences in the implementation of the estimator between this work and Ref. [11] are

outlined in Appendix A, while the consequent differences in temperature results can be seen by comparing Table I with table I of Ref. [11] (though the differences are not significant). Here we present a condensed description of our estimator (the full details are in Appendix C of [5]).

We note that our estimator is essentially identical to that of Ref. [2] and can also be rewritten in terms of BiPoSH coefficients [35, 36]; however, the physical motivation for this approach comes from Ref. [31], where general cosmological parameter modulations were explored. Our implementation to deal with masking and noise uses an inverse-variance filter on the spherical harmonic coefficients that optimally account for the masking, as used in Refs. [5, 37, 38].

B. Full-sky, noise-free case

From Eq. (11) it is clear that the multipole covariance can be decomposed into an isotropic part and a small anisotropic part proportional to ΔX_M . In other words, we can make the identification $C_{\ell m \ell' m'} = C_I + C_A$, with C_I being the first term on the right hand side of Eq. (11) and C_A being the second term. The inverse covariance matrix can then be written as $C_I^{-1} - C_I^{-1} C_A C_I^{-1}$ (to linear order in the anisotropy). The best-fit ΔX_M values are given by

$$\Delta X_M = \frac{d^\dagger C_I^{-1} \partial C_A / \partial \Delta X_M C_I^{-1} d}{\text{Tr} [C_I^{-1} \partial C_A / \partial \Delta X_M C_I^{-1} \partial C_A / \partial \Delta X_M]}, \quad (20)$$

for multipole vector d . These can be written more explicitly as

$$\begin{aligned} \Delta X_0 &= \frac{6 \sum_{\ell m} \delta C_{\ell \ell+1} C_\ell^{-1} C_{\ell+1}^{-1} A_{\ell m} a_{\ell m}^* a_{\ell+1 m}}{\sum_{\ell} \delta C_{\ell \ell+1}^2 C_\ell^{-1} C_{\ell+1}^{-1} (\ell+1)}, \quad (21) \\ \Delta X_{+1} &= \frac{6 \sum_{\ell m} \delta C_{\ell \ell+1} C_\ell^{-1} C_{\ell+1}^{-1} B_{\ell m} a_{\ell m}^* a_{\ell+1 m+1}}{\sum_{\ell} \delta C_{\ell \ell+1}^2 C_\ell^{-1} C_{\ell+1}^{-1} (\ell+1)}, \quad (22) \end{aligned}$$

and $\Delta X_{-1} = -\Delta X_{+1}^*$. We note that Eq. (20) is completely general and can be used to examine modulation of any kind (i.e., beyond simple dipolar modulation). The cosmic variance of the modulation amplitude estimator is given by

$$\sigma_X^2 \equiv \langle |\Delta X_M|^2 \rangle = 12 \left(\sum_{\ell} (\ell+1) \frac{\delta C_{\ell \ell+1}^2}{C_\ell C_{\ell+1}} \right)^{-1}. \quad (23)$$

As we mentioned in Sec. II A, we strictly only consider values of the modulation amplitude ($A_{\mathcal{R}}$, Δn_s , A_t , or $A_{\mathcal{I}}$) less than unity. Note, however, that the $\mathcal{O}(\Delta X^2)$ terms which were dropped in the multipole covariance, Eq. (11), couple ℓ with ℓ and $\ell \pm 2$. Therefore the estimator, Eqs. (21) and (22), will be insensitive to them. In other words, our approach will correctly recover modulation amplitudes as large as our cutoff of unity: we have no need to restrict to small ΔX .

C. Realistic skies

The estimators presented in Sect. III B are only adequate for full sky coverage with no noise. In this subsection we show how we include the effects of masking and noise in the data.

The combination of $C_I^{-1} d$ in Eq. (20) is suggestive that we should apply an inverse-covariance filter to the data. This is exactly what we do. The effects of masking are readily dealt with by employing inverse-variance filtering to the data, as described in Refs. [37, 38]. Pixels within the mask are given infinite variance and thus are given zero weight, which optimally accounts for masking effects. The effects of inhomogeneous noise could also readily be handled by including its variance contribution in the inverse-variance filter. However, we have not included these effects, which means we will have a slightly suboptimal though still *unbiased* estimate. Residual effects not captured by our approach (e.g. inhomogeneous noise) are handled by subtracting a mean field term, derived from simulations with the same foreground and noise properties as the data. We note that this same approach has been used for lensing estimators in Refs. [37, 38] and specifically for temperature dipole modulation in Refs. [5, 11].

The estimator, Eqs. (21)–(22), then becomes

$$\tilde{X}_0^{WZ} = \frac{6 \sum_{\ell m} \delta C_{\ell \ell+1}^{WZ} A_{\ell m} S_{\ell m \ell+1 m+M}^{(WZ)}}{\sum_{\ell} (\delta C_{\ell \ell+1}^{WZ})^2 (\ell+1) F_{\ell}^{(W)} F_{\ell+1}^{(Z)}}, \quad (24)$$

$$\tilde{X}_{+1}^{WZ} = \frac{6 \sum_{\ell m} \delta C_{\ell \ell+1}^{WZ} B_{\ell m} S_{\ell m \ell+1 m+M}^{(WZ)}}{\sum_{\ell} (\delta C_{\ell \ell+1}^{WZ})^2 (\ell+1) F_{\ell}^{(W)} F_{\ell+1}^{(Z)}}, \quad (25)$$

with

$$S_{\ell m \ell' m'}^{WZ} \equiv W_{\ell m}^* Z_{\ell' m'} - \langle W_{\ell m}^* Z_{\ell' m'} \rangle. \quad (26)$$

Here, $WZ = TT, TE, EE$; $W_{\ell m}$ and $Z_{\ell m}$ are inverse-covariance filtered data; $F_{\ell}^W \simeq \langle W_{\ell m} W_{\ell m}^* \rangle$; and the last term on the right-hand-side of Eq. (26) denotes the mean-field correction (details including the precise form of F_{ℓ}^W can be found in Appendix A.1 of Ref. [38] and Appendix A of this paper). The parentheses in the superscripts indicate symmetrization over the enclosed variables.

The estimators of Eqs. (24)–(25) can be combined with inverse-variance weighting over all data combinations (TT , TE , EE) to obtain a combined minimum-variance estimator, given by

$$\Delta \tilde{X}_M = \frac{\sum_{WZ} \Delta \tilde{X}_M^{WZ} (\sigma_X^{WZ})^{-2}}{\sum_{WZ} (\sigma_X^{WZ})^{-2}}. \quad (27)$$

Here we calculate the variance from the scatter of simulations, although they agree closely with the Fisher errors given in Ref. [5].

IV. RESULTS

A. Temperature only

In this section we show constraints using *Planck* temperature data only. Specifically, we use the SMICA 2015 temperature solution, one of four *Planck* component-separation methods [39], all of which produce very similar results [5]. The temperature data are evaluated up to a maximum multipole $\ell_{\max} = 1000$ (no significant difference was found when extending to higher multipoles), with the exception of the modulated n_s model, which uses $\ell_{\max} = 2000$.

Fig. 1 shows the posteriors of the modulation parameters for our adiabatic models. Results for the tanh model have already been commented on in [11]; here we simply reiterate that the model is (unsurprisingly) not constrained well with temperature alone. The pile-up of the posterior at low modulation amplitudes (present for all models, though most notably for the adiabatic power-law model) is a volume effect that arises due to our choice of prior, which expects uniform posteriors for the k -space parameters ($k_c, \Delta \ln k, k_*, n_s^{\text{lo}}$) for statistically isotropic data.

The best-fit modulation parameters for all models are presented in Table I. We see that the modulation amplitudes required for the tensor and isocurvature models exceed unity, i.e., the best fits have $A_t, A_{\mathcal{I}} > 1$. This suggests that, for the case of tensor and isocurvature isotropic contributions at the current upper limits ($r_{0.05} = 0.07$ and $\alpha = 0.04$), maximal modulation (i.e., modulation amplitude unity) is insufficient to produce the observed temperature asymmetry. For this reason we do not discuss these models further here. This result will be addressed more quantitatively in [30]. Note that this conclusion for a specific isocurvature model was originally made in [27][46].

Parameter	tanh	ad.-PL	n_s -grad	tensors	isocurvature
$10^3 k_c [\text{Mpc}^{-1}]$	7.45
$\Delta \ln k$	0.5
n_s^{lo}	...	-0.09
$k_* [\text{Mpc}^{-1}]$	0.10
ΔX	-0.065	-0.457	-0.011	-2.2	-1.2
ΔY	-0.044	-0.566	-0.008	-2.0	-1.0
ΔZ	-0.035	-0.499	-0.004	-1.3	-0.8
$A_{\mathcal{R}}$	0.086	0.882
Δn_s	0.014
A_t	3.3	...
$A_{\mathcal{I}}$	1.8
$l [^\circ]$	214	231	214	221	221
$b [^\circ]$	-24	-34	-17	-24	-28

TABLE I: Best-fit modulation parameters for the *Planck* temperature data, given the models described in Sect. II.

In Fig. 2 we compare the Λ CDM power spectra to the asymmetry spectra, AC_ℓ^{lo} , for the temperature best-fit

modulation parameters given in Table I, for each of our models. Note that the best-fit TT asymmetry spectra correspond very roughly to 5% modulation in amplitude out to $\ell \simeq 60$, as expected from the previous ℓ -space analyses of the asymmetry.

It is worth reiterating that none of these models are currently favoured over base Λ CDM: the goodness of fit of these models to the asymmetry (and isotropic) data is discussed in detail in [30]. Hence the interest here in pursuing polarization data to improve constraints and test for a physical origin to the asymmetry.

B. Including polarization

1. E vs. T asymmetry spectra

We claimed in Sec. I that it was not reasonable to take the observed multipole-space temperature asymmetry, e.g., 6% asymmetry to $\ell = 65$, and predict a 6% asymmetry in E to $\ell = 65$. We demonstrate this explicitly in this subsection, using the tanh model as an example. First, in Fig. 3 we illustrate the cosmic variance [calculated via Eq. (23)] for a measurement of the amplitude of tanh modulation versus cutoff scale k_c , for $\Delta \ln k = 0.01$ (which corresponds closely to a step function in k -space, with modulation only for $k < k_c$). It is clear that for most values of k_c , the cosmic variance is considerably smaller for an EE measurement than for a TT measurement. In particular, this applies around the best-fit value, $k_c = 7.45 \times 10^{-3} \text{ Mpc}^{-1}$, where the EE standard deviation is smaller by a factor of nearly two than the TT value. This is in stark contrast to the naive ℓ -space expectation, where identical modulation cutoffs for TT and EE leads to identical cosmic variance. However, we can also see that there are some values of k_c for which the EE cosmic variance is comparable to or even worse than the TT value.

To help understand these differences between TT and EE , we plot in Fig. 4 asymmetry spectra $C_\ell^{T,\text{lo}}$ and $C_\ell^{E,\text{lo}}$ for the tanh model with $\Delta \ln k = 0.01$. For the case $k_c = 7.45 \times 10^{-3} \text{ Mpc}^{-1}$ (i.e., the best-fit value), we can see that the asymmetry spectra differ substantially between T and E (note that this effect is also visible in figure 1 of [22]). In particular, we predict substantially larger modulation, and hence lower cosmic variance, in E than in T , since $C_\ell^{E,\text{lo}} > C_\ell^{T,\text{lo}}$ for all ℓ . The reason for this is that the transfer functions from k - to ℓ -space are narrower for E than for T , and hence the step is better resolved in E . On the other hand, for the case $k_c = 2 \times 10^{-2} \text{ Mpc}^{-1}$ some fine k -space structure (a dip in this case) is resolved by polarization and leads to lower asymmetry power for EE and hence larger cosmic variance. This illustrates the importance of working in k -space rather than ℓ -space when testing models for modulation.

Importantly, these results imply that an ideal polarization measurement can improve on the TT modulation amplitude measurement error considerably better

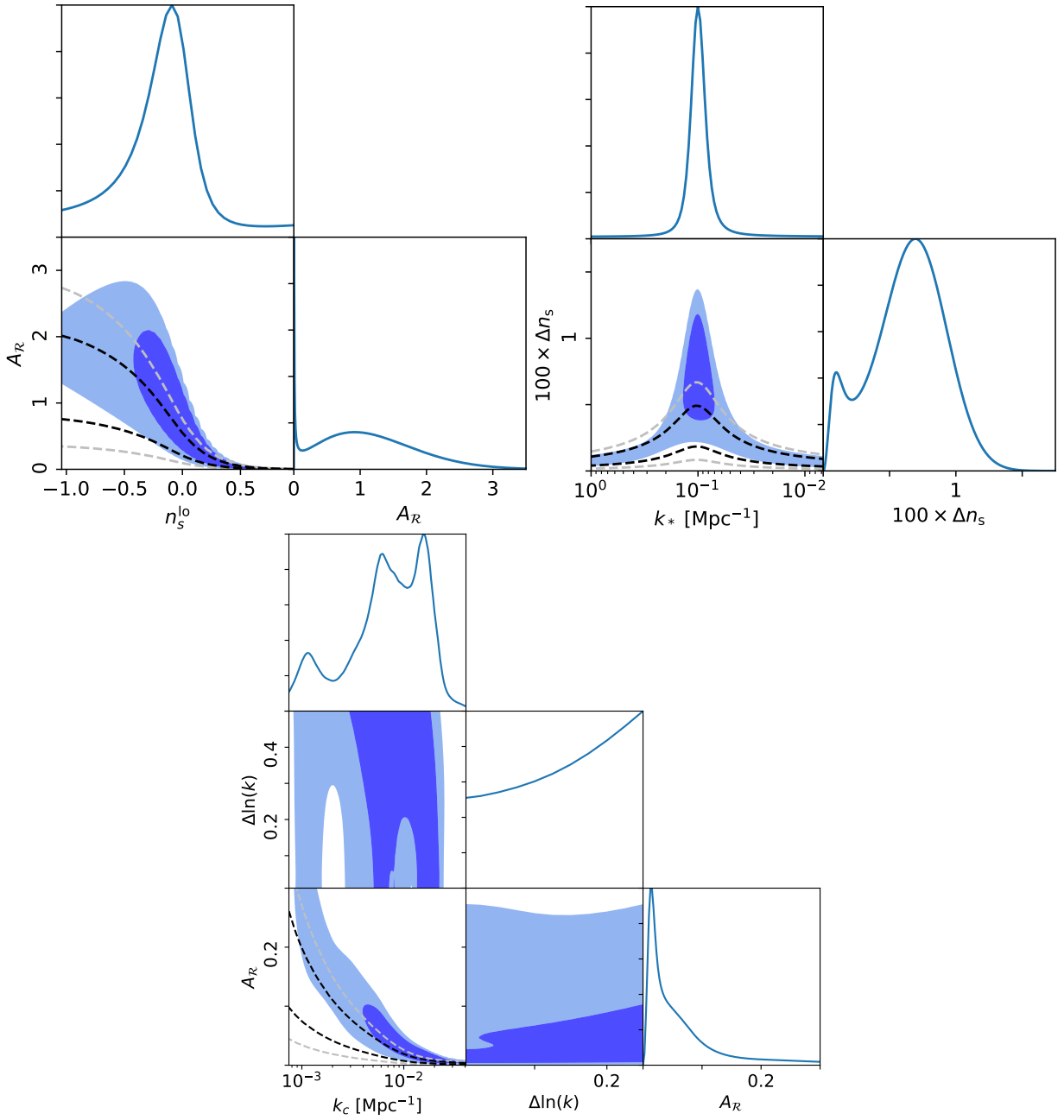


FIG. 1: Marginalized posteriors for the adiabatic power-law (top left triangle plot), n_s gradient (top right), and tanh (bottom) models, using *Planck* temperature data only. Dark and light blue regions enclose 68% and 95% of the likelihood, respectively. The black dashed curves represent the theoretical distributions of the parameters coming solely from cosmic variance in statistically isotropic skies.

than the naive ℓ -space expectation of $\sqrt{2}$. In Fig. 5 we show the expected improvement to the error bar on the amplitude of modulation in a known direction (σ_X) when adding *Planck* or cosmic-variance-limited polarization to *Planck* temperature, as a function of the modulation parameters. (Recall that for temperature we use $\ell_{\max} = 2000$ for the n_s gradient model and $\ell_{\max} = 1000$ for all others.) For the tanh model the dependence on $\Delta \ln k$ is quite weak and so we have averaged over it and only show the dependence on k_c . We can see that

even with *Planck* polarization (blue curves), there are parameter values for which the addition of polarization decreases the error bar by more than the naive expectation of $\sqrt{2}$. This, again, is due to the difference in the k -to- ℓ transfer functions between polarization and temperature. That is, for the same $\mathcal{P}^{\text{lo}}(k)$ modulation, polarization modes are more strongly modulated (on many scales) than temperature, as we saw in Fig. 4. It is also worth noting that the variations in improvement follow the peak structure of the EE power spec-

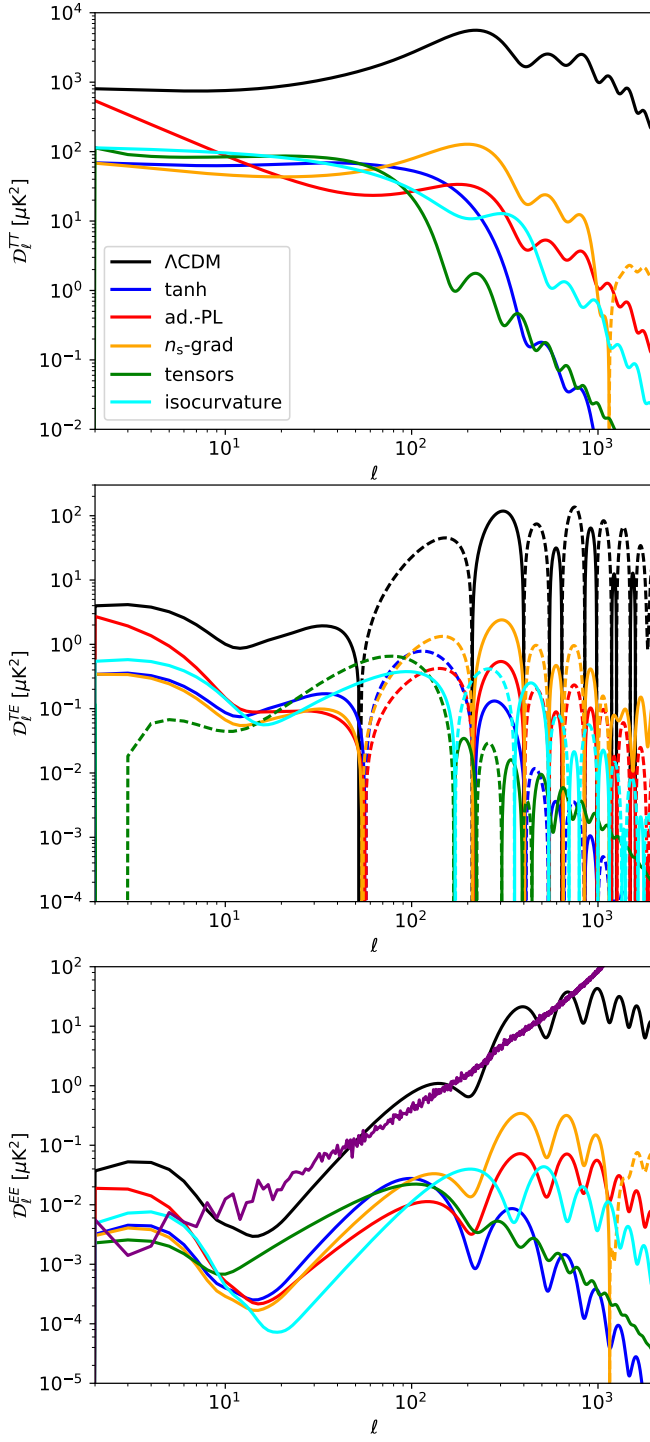


FIG. 2: Λ CDM power spectra for TT , TE , and EE (top to bottom panels) compared to the best-fit asymmetry spectra, AC_ℓ^{lo} , to the *Planck* temperature data (see Table I), for the various models. The purple curve in the bottom panel is the noise power spectrum for a single FFP8 noise realization. The best-fit TT asymmetry spectra give several-percent-level asymmetry for $\ell \lesssim 100$, as expected. Here $D_\ell \equiv \ell(\ell+1)C_\ell/(2\pi)$.

tra, i.e., the first three peaks that are above the noise level in Fig. 2. This is most clearly evident with the

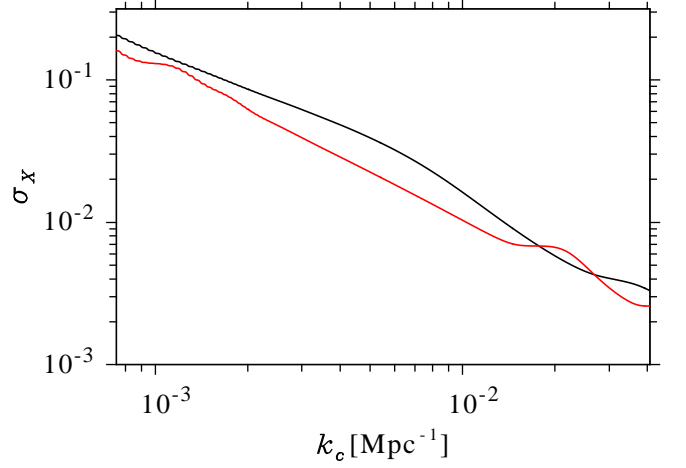


FIG. 3: Cosmic variance for a measurement of the amplitude of modulation for the tanh model (with $\Delta \ln k = 0.01$) for TT (black curve) and EE (red). Polarization does considerably better than the naive ℓ -space expectation of identical cosmic variance for TT and EE .

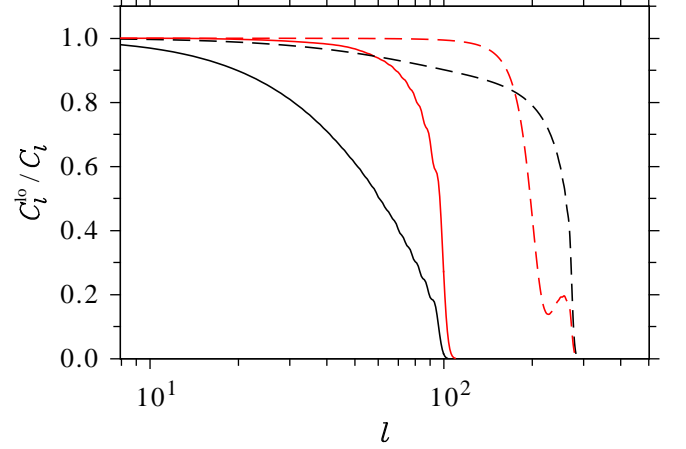


FIG. 4: Asymmetry spectra C_ℓ^{lo} for temperature (black curves) and E -mode polarization (red) for the tanh model of Sec. II B 1, with $\Delta \ln k = 0.01$ and $k_c = 7.45 \times 10^{-3} \text{ Mpc}^{-1}$ (solid curves) and $k_c = 2 \times 10^{-2} \text{ Mpc}^{-1}$ (dashed). The same physical k -space modulation produces substantially more modulation of E than of T for the lower k_c value, and conversely for the higher k_c value.

tanh model. The expected improvement when adding cosmic-variance-limited polarization exceeds a factor of two for some models and parameter ranges, substantially exceeding the naive value of $\sqrt{2}$.

2. Constraints

We cross-check and validate our method through the use of FFP8 component-separated CMB + noise simulations [24], masked appropriately using the *Planck* 2015 common mask for polarization, with $f_{\text{sky}} = 0.75$. For our cosmic-variance-limited results we remove the noise

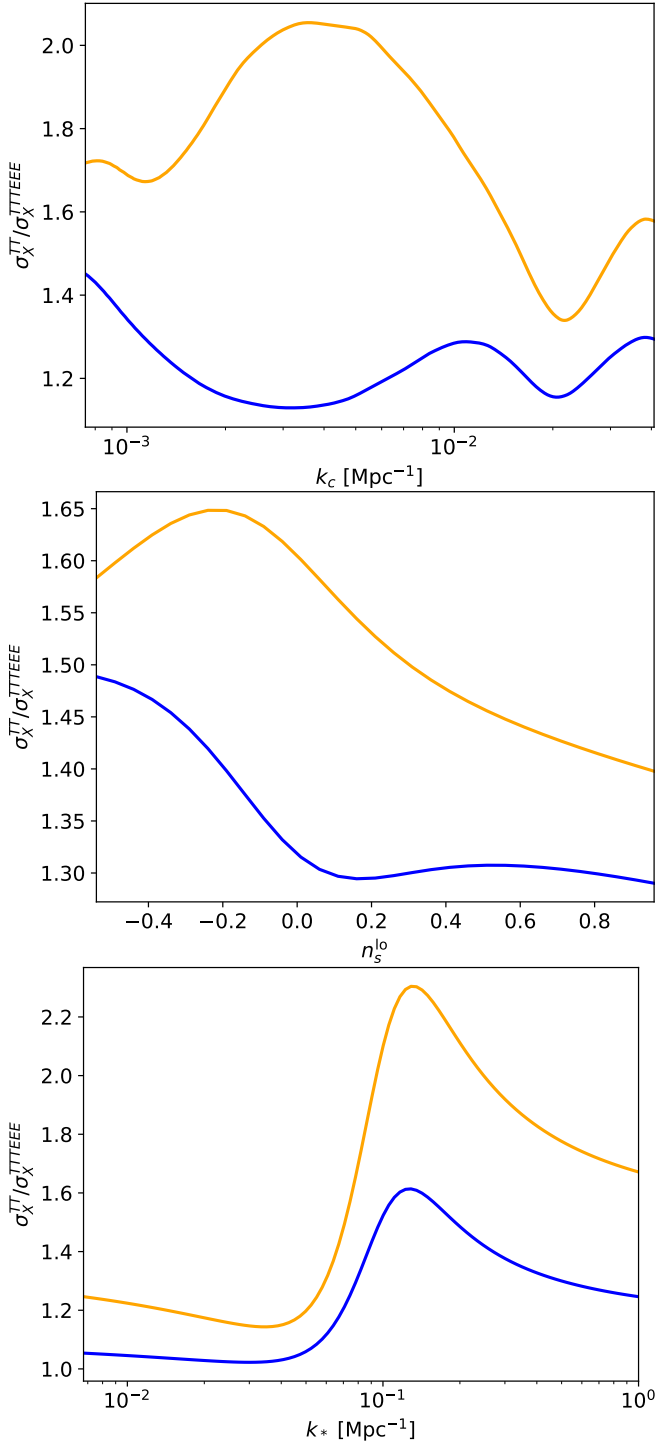


FIG. 5: Improvement in the error bar for a measurement of the amplitude of modulation for the tanh, adiabatic power-law, and n_s gradient models (top to bottom panels), assuming that the modulation direction is known, when *Planck* (blue curves) or cosmic-variance-limited (orange) simulated polarization data (to $\ell_{\text{max}} = 1000$) are added to *Planck* temperature. The dependence on k_c for the *Planck* case tanh model follows the peak structure of the EE power spectra relative to the noise (see Fig. 2, bottom) and can exceed the naive expectation of $\sqrt{2}$.

in the polarization simulations and apply *no* mask. For all models we examine our polarization simulations up to a maximum multipole $\ell_{\text{max}} = 1000$. Throughout we will consider adding statistically isotropic or anisotropic polarization to *Planck* temperature data. In both scenarios we will use the same set of FFP8 simulations, modified to either include the appropriate temperature-polarization correlation with the *given* temperature data (for the case of statistically isotropic polarization, see Appendix B 1), or to include the appropriate modulation for the specific model and parameters considered (see Appendix B 2).

First we consider the case that the asymmetry does not have a physical origin and is simply due to fluctuations consistent with cosmic variance. In this case the polarization must be treated as statistically isotropic (apart from the necessary T - E correlation). We apply Bayesian parameter fitting to the combination of temperature data and polarization simulations (treated as if they were data). In Figs. 6–8 we show the marginalized posteriors of the modulation parameters for temperature data alone (in black) and when adding statistically isotropic polarization data averaged over 500 simulations and shown by the blue solid and dashed curves for *Planck* and cosmic-variance-limited polarization, respectively. In general the addition of isotropic polarization data will act to spread out the posteriors with respect to the temperature-only constraints. However, we find that the addition of *statistically isotropic* polarization data increases the significance of a $\geq 3\sigma$ temperature result (here we mean with respect to the amplitude parameter only) roughly 30% or 20% of the time for *Planck* or cosmic-variance-limited polarization, respectively. This is mainly due to the initial weakness of the temperature signal. Therefore, we urge caution when interpreting the addition of polarization data to temperature.

Next we consider the case that the asymmetry is due to a real modulation, so the polarization will be statistically anisotropic with a precise form determined by the k -space modulation model. We generate modulated polarization simulations (modulated with the temperature best-fit parameters given in Table I) to combine with the temperature data to forecast the type of constraints we expect to see in *Planck* and cosmic-variance-limited data if the modulation is real. We modify the existing FFP8 simulations following the procedure in Appendix B 2.

Results are also summarized in Figs. 6–8, where the addition of modulated polarization is shown with the orange solid and dashed curves for *Planck* and cosmic-variance-limited polarization, respectively. The curves plotted are the mean posteriors averaged over 500 simulations. We see that in general the addition of polarization makes the data more constraining. However, these figures do not show how often we should expect to be able to distinguish modulated polarization from statistically isotropic polarization, which will necessarily be model dependent. We will be more quantitative about this in the following subsection.

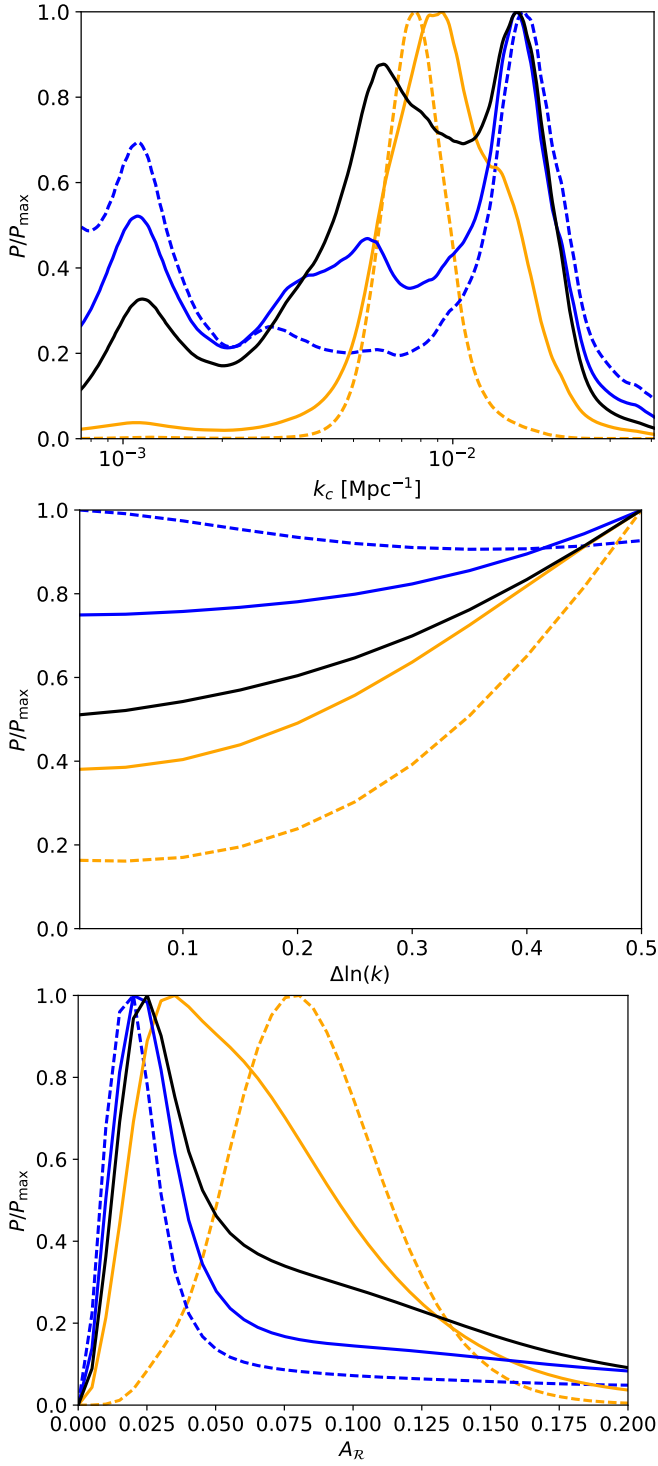


FIG. 6: Posteriors for k_c , $\Delta \ln k$, and A_R (top to bottom panels) for the tanh model for temperature alone (black curves) and temperature with isotropic (blue) and modulated (orange) polarization simulations for the model parameters in Table I. The posteriors using polarization have been averaged over 500 polarization realizations. Solid curves refer to *Planck* polarization, while dashed curves refer to cosmic-variance-limited polarization. The parameter k_c is typically somewhat more constrained in the modulated than in the isotropic polarization case, but cosmic variance is still significant.

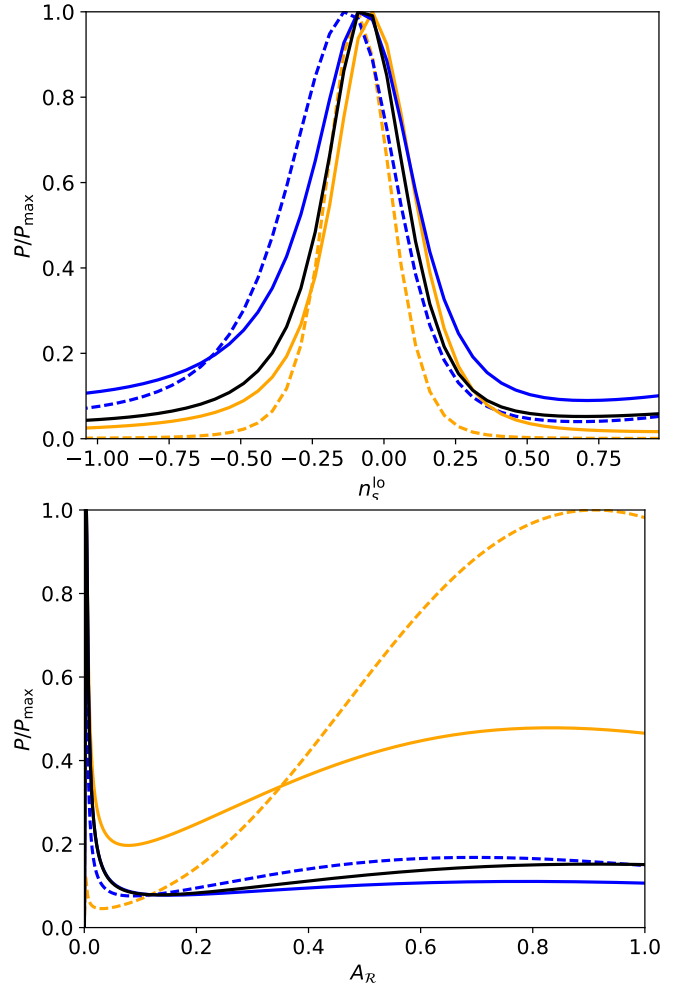


FIG. 7: Posteriors for n_s^{lo} and A_R (top and bottom panels, respectively) for the adiabatic power-law model for temperature alone (black curves) and temperature with isotropic (blue) and modulated (orange) polarization simulations for the parameters given in Table I. The posteriors using polarization have been averaged over 500 polarization realizations. Solid curves refer to *Planck* polarization while dashed curves refer to cosmic-variance-limited polarization.

C. Distinguishing modulated from isotropic polarization

If the signal seen in temperature has a physical cause then it is clearly too low in signal-to-noise to definitively distinguish from cosmic variance fluctuations. With the addition of polarization, however, we can assess how well one could distinguish statistically anisotropic from statistically isotropic data. With this in mind we define the quantity \hat{O}_{jk} as the ratio of maximum likelihood of model j over model k . For definiteness we will order the models in the following way:

0. Λ CDM;
1. tanh model;
2. adiabatic power-law model;

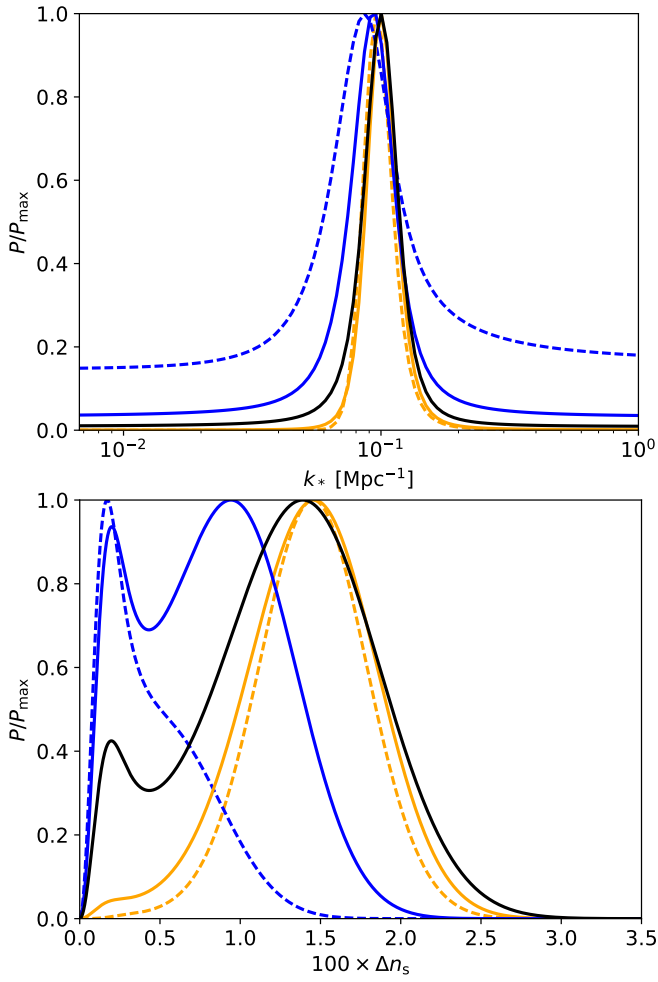


FIG. 8: Posteriors for k_* and Δn_s (top and bottom panels, respectively) for the n_s gradient model for temperature alone (black curves) and temperature with isotropic (blue) and modulated (orange) polarization simulations, for the parameters given in Table I. The posteriors using polarization have been averaged over 500 polarization realizations. Solid curves refer to *Planck* polarization while dashed curves refer to cosmic-variance-limited polarization.

3. n_s gradient.

For a modulation model j , the maximum likelihood is proportional to $\exp[A^2/(2\sigma_X^2)]_{\max}$, whereas for Λ CDM, it is proportional to $\exp[-A^2/(2\sigma_X^2)]_{\max}$. Therefore we can compute \hat{O}_{j0} as

$$\hat{O}_{j0} = \frac{\{\exp[A^2/(2\sigma_X^2)]\}_{\max}}{\{\exp[-A^2/(2\sigma_X^2)]\}_{\max}}. \quad (28)$$

Note that Eq. (28) is related to the often used odds ratio for Bayesian model comparison, but without the Occam penalty factor [40]. For this reason the meaning of the *absolute* value of \hat{O}_{j0} is irrelevant, though the *relative* value between different data (modulated or statistically isotropic) is valuable. We will thus use \hat{O}_{j0} as a proxy for distinguishing modulated data from statistically isotropic data by comparing to statistically isotropic or modulated simulations.

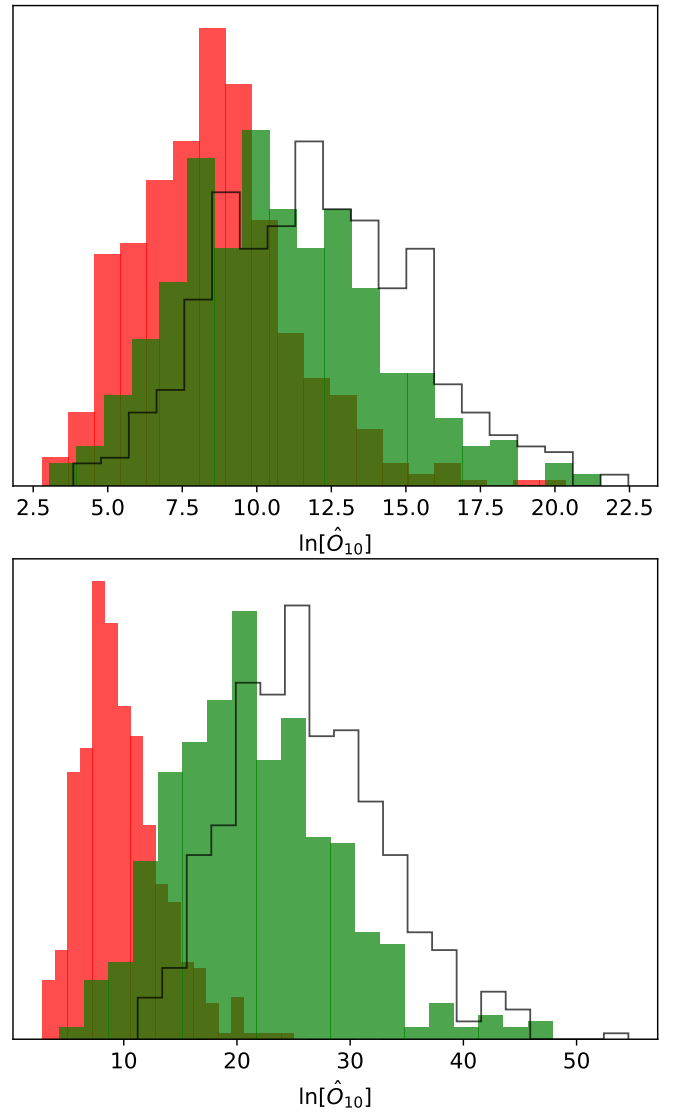


FIG. 9: Histogram of the logarithm of \hat{O}_{j0} [defined by Eq.(28)] for the tanh model using the *Planck* temperature data with 500 realizations of statistically isotropic (red) or modulated (black outlines and green) polarization as described in the text. The top panel uses *Planck* polarization, while the bottom uses cosmic-variance-limited polarization. Large values relative to the isotropic histograms indicate that the modulation model should be preferred over Λ CDM.

For the data we will choose to add either statistically isotropic or modulated polarization to the existing *Planck* temperature data. The results are shown in Figs. 9–11, where the relation between the colours and the type of simulations are as follows:

- red statistically isotropic polarization added to temperature data;
- green modulated polarization added to temperature data, where the modulation parameters are determined by randomly sampling the full likelihood of the temperature data;
- black modulated polarization added to tempera-

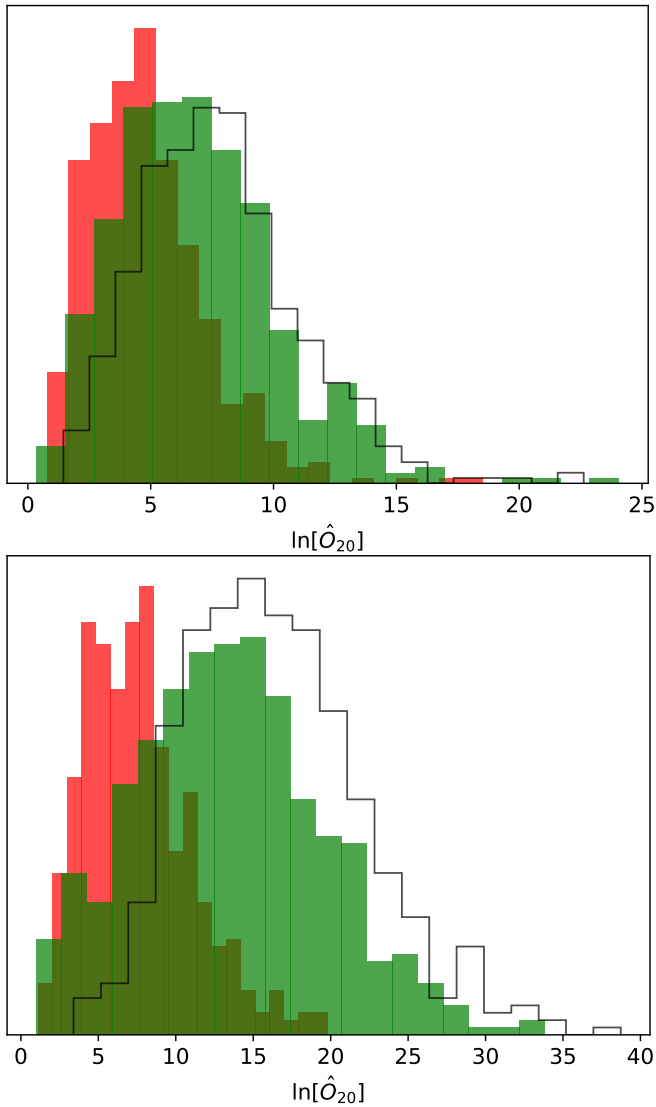


FIG. 10: As in Fig. 9 except for the adiabatic power-law model.

ture data using the best-fit modulation parameters from Table I.

The figures show the histogram of the logarithm of \hat{O}_{j0} . Large values of \hat{O}_{j0} relative to the isotropic-polarization simulations indicate that the modulation model should be preferred over Λ CDM, and indeed the modulated simulations are clearly shifted to the right of the statistically isotropic simulations, with the black histograms further to the right than the green. A large overlap in the distributions would indicate that it will be difficult to distinguish modulated from statistically isotropic data using polarization.

We would like to assess the probability of a detection of modulation assuming that the polarization data are modulated as predicted by temperature. In Table II we indicate for each model the probability that \hat{O}_{j0} is greater than that of 95% of isotropic (red) simulations—we will loosely refer to this as a “ 2σ ”-detection. The

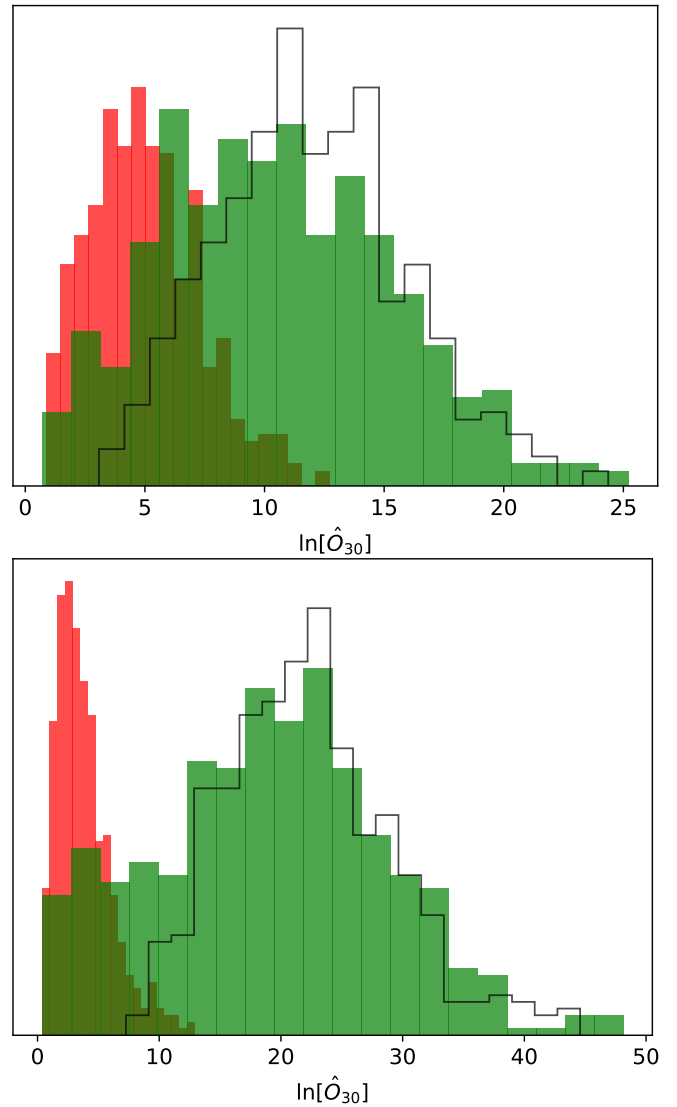


FIG. 11: As in Fig. 9 except for the n_s gradient model.

“best-fit” values refer to polarization modulated with the temperature best-fit parameters from Table I. In this case the probability of a 2σ detection with *Planck* polarization ranges from 27% for the adiabatic power-law model to 75% for the n_s gradient model. For cosmic-variance-limited polarization these probabilities increase substantially, reaching 99% for the n_s gradient model. However, as the “sampling” columns in Table II show, when we sample the modulation parameters from the full temperature posteriors, the probabilities are reduced.

We see that even in the optimistic scenario that the true modulation parameters are given by the best-fit values of the temperature likelihood, *Planck* has a low probability of distinguishing this from statistically isotropic data. The exception is the case of the n_s gradient model, which has a large tail out to very large \hat{O}_{30} values even when simulated *Planck* polarization data are used. The situation improves considerably when cosmic-variance-limited polarization is used, with the tanh and n_s -grad models being almost guaranteed to be detected in the

Model	<i>Planck</i>		CV-limited	
	best fit	sampling	best fit	sampling
tanh	37%	23%	94%	75%
ad.-PL	27%	20%	63%	45%
n_s -grad	75%	58%	99%	84%

TABLE II: Probability of a “ 2σ ”-detection (as defined in Sect. IV C) of a real modulation as described by the model in the first column given modulated *Planck* or cosmic-variance-limited polarization. The “best fit” columns refer to modulating polarization with the best-fit values from the temperature data (see Table I). The “sampling” columns refer to modulating polarization using parameters chosen by randomly sampling the full likelihood of the temperature data. The latter values are a more conservative approach to how the polarization might be modulated and thus give smaller probabilities of detection.

scenario that the true modulation model is given by the best-fit temperature parameters. These large probabilities are diminished when we consider the case that polarization is instead modulated with parameters randomly sampling the likelihood of the temperature data, which is not constrained well. However, these “sampling” probabilities are the best statements we can make about detectability of modulation given the temperature signal, and should be considered as our most conservative results.

V. DISCUSSION

In this paper we have applied to CMB polarization the formalism of Ref. [11], which describes the effect of a spatially linear modulation with arbitrary scale dependence. We have used the statistically isotropic temperature and polarization simulations provided by the *Planck* collaboration to estimate the decrease in uncertainty in the modulation parameters when polarization is added. We have also generated asymmetric polarization simulations to see how well we could test the possibility that the modulation is a real, physical effect. We have characterized the probability of a “ 2σ ” detection of our dipolar modulation models (introduced in Sect. II) when adding *Planck* or cosmic-variance-limited polarization data under the following important assumptions: 1) The modulation model is correct (i.e., the primordial fluctuations are actually modulated according to the model in question); 2) the polarization data are free of any relevant systematic effects; and 3) the effective sky coverage is similar to what is available for the *Planck* temperature data (though our noiseless polarization simulations use the full sky). We found that, for the case of *Planck* polarization, we expect a probability of anywhere from 20% to 75% for such a 2σ detection. For cosmic-variance-limited polarization, the probability increases to the range 45% to 99%. We have shown that these results are considerably stronger than a simple ℓ -space analysis would predict, due to the ability of polarization to resolve k -space

detail more sharply than temperature.

Our results are clearly strongly model dependent, with the n_s gradient model being the most likely to be ruled out or confirmed. This is due to the distinct scale dependence for this model, with substantial modulation at very small scales. This suggests that extending the polarization data to $\ell_{\max} = 2000$ would provide a decisive test of this model.

Furthermore, we found that the probability that adding statistically isotropic polarization spuriously *increases* the significance of a $\geq 3\sigma$ signal (with respect to the amplitude) is 30% or 20% for *Planck* or cosmic-variance-limited polarization, respectively. This probability is large due to the moderate strength of the modulation signal in temperature. Therefore caution is warranted if polarization is found to increase the significance of the temperature signal.

For a spatially linear modulation (as with our models) the addition of polarization is our best short-term hope at detecting such a signal. This is because in practice the surface of last scattering is the furthest distance we have access to and thus perturbations sourced there would be modulated with a higher amplitude than observables such as lensing [11] or integrated Sachs-Wolfe effect [30], for example. In spite of the poor ability of *Planck* polarization to address modulation, all is not lost, as a CMB-S4 [41] project or CORE [42] would reach noise levels such that E -mode polarization is essentially cosmic-variance limited. This should provide a strong indication of the true nature of the dipole asymmetry signal, at least for some models (recall the final two columns of Table II). Farther into the future, 21 cm measurements of the dark ages ($z \gtrsim 30$) may be able to help in constraining the dipole modulation models considered here due to the vastly larger number of modes accessible to three-dimensional probes.

Acknowledgements

This research was supported by the Canadian Space Agency and the Natural Sciences and Engineering Research Council of Canada.

Appendix A: Filtering

In Ref. [11] a simplified noise model was used when treating the temperature data. The model did not account for variations in the noise level due to the *Planck* scanning strategy, or scale-dependence of the noise power, or foreground signal. Not accounting for these effects was deemed adequate due to the noise power being subdominant on the scales probed. However, for polarization this is not the case. Here we describe our approach to account for the scale dependence of the noise and foreground power (as used similarly in Ref. [38]). The corrections below are applied after the filtering process and are the cause of the small differences between

the temperature results here and those in Ref. [11].

Our starting point will be filtered data as in [11], denoted here as $s_{X,\ell m}$, where $X = T$ or E . We multiply these by a quality factor Q_ℓ^X to obtain filtered data that are closer to optimal, defining

$$X_{\ell m} = Q_\ell^X s_{X,\ell m}. \quad (\text{A1})$$

The choice of Q_ℓ^X is determined by the following two requirements:

$$F_\ell^X = \frac{Q_\ell^X}{C_\ell^{XX} + N_\ell^{XX}}, \quad (\text{A2})$$

$$F_\ell^X = \frac{f_{\text{sky}}^{-1}}{2\ell+1} \sum_m |X_{\ell m}|^2. \quad (\text{A3})$$

Here $f_{\text{sky}} = \sum_p M_p / N_{\text{pix}}$, where M_p is the map in pixel space and N_{pix} is the total number of pixels. Further details can be found in Appendix A.1 of Ref. [38].

Appendix B: Simulating modulation parameters

1. Isotropic estimates

The FFP8 simulations require modification in order to combine isotropic polarization data with temperature data. This is because the polarization simulations are not correlated with temperature data in the way that the true polarization data are. While this is a small correction, we describe below how we account for it.

For each simulation to be included with the temperature data we modify the modulation estimator (\tilde{X}_M^{WZ}) in the following way:

$$\tilde{X}_M^{WZ \text{ cor}} = \tilde{X}_M^{WZ} + \tilde{X}_M^{TT, \text{data}} \frac{\text{Cor}(\tilde{X}_M^{WZ}, \tilde{X}_M^{TT})}{\text{Var}(\tilde{X}_M^{TT})}. \quad (\text{B1})$$

The correlation and variance are estimated with the statistically isotropic FFP8 simulations. Note that this procedure only modifies the values of the estimators (the \tilde{X}_M 's) and *not* the CMB simulations themselves. This provides a significant computational speed-up when analyzing a large number of simulations.

If the \tilde{X}_M 's are Gaussian (which we verify to be true with our simulations) then this approach is exact and amounts to simply shifting the mean of \tilde{X}_M^{TE} and \tilde{X}_M^{EE} by an amount given by the *fixed* temperature data [23].

2. Anisotropic estimates

In the appendix of Ref. [2] it was demonstrated how to generate anisotropic maps from isotropic ones. Such an algorithm is convenient, but can be computationally expensive when scanning over many different anisotropic models. In this Appendix we will demonstrate our strategy for quickly generating modulated *estimates* (\tilde{X}_M 's) by using isotropic estimates (thus skipping the step of generating maps, filtering them, and computing estimates from them).

For simplicity we will assume that we want to generate modulation in the $+\hat{z}$ -direction; however, a general direction can be implemented by simply breaking the direction into components. The following will make use of binned versions of the estimators of Eqs. (24)–(25). These can be written as

$$\tilde{X}_{0,\ell}^{WZ} = \frac{6 \sum_m A_{\ell m} S_{\ell m \ell+1 m}^{(WZ)}}{\delta C_{\ell \ell+1}^{WZ} (\ell+1) F_\ell^{(W)} F_{\ell+1}^{(Z)}}. \quad (\text{B2})$$

Thus we see that at each multipole an estimate of the amplitude (and direction) can be made. If we want to generate an estimate of an anisotropic simulation we can modify an estimate of an isotropic simulation in the following way. First we compute Eq. (B2) for an isotropic simulation at the desired modulation parameters (e.g., $\tilde{p}_i = \{\tilde{k}_c, \Delta \ln \tilde{k}\}$ for the tanh model), which implies a particular anisotropic power spectrum $\tilde{\delta C}_{\ell \ell+1}^{WZ}$. Then an anisotropic binned estimator can be obtained as

$$\tilde{X}_{0,\ell}^{WZ \text{ ani}}|_{\tilde{p}_i} = \tilde{X}_{0,\ell}^{WZ \text{ iso}}|_{\tilde{p}_i} + \tilde{A}, \quad (\text{B3})$$

where \tilde{A} is the desired amplitude of modulation. The full estimator, Eqs. (24)–(25), for a general modulation model ($\delta C_{\ell \ell+1}$) can be recovered by

$$\tilde{X}_0^{WZ \text{ ani}} = \frac{\sum_\ell \tilde{X}_{0,\ell}^{WZ \text{ ani}}|_{\tilde{p}_i} \tilde{\delta C}_{\ell \ell+1}^{WZ} \delta C_{\ell \ell+1}^{WZ} (\ell+1) F_\ell^{(W)} F_{\ell+1}^{(Z)}}{\sum_\ell (\delta C_{\ell \ell+1}^{WZ})^2 (\ell+1) F_\ell^{(W)} F_{\ell+1}^{(Z)}}. \quad (\text{B4})$$

Appendix C: Detection and removal of aberration

Aberration due to our velocity relative to the CMB frame adds a term to the CMB temperature multipole covariance given by [43]

$$\langle a_{\ell m} a_{\ell+1 m}^* \rangle = -\beta A_{\ell m} [(\ell+2)C_{\ell+1} - \ell C_\ell]. \quad (\text{C1})$$

Here the $a_{\ell m}$'s are defined in a coordinate system where the dipole direction, $(l, b) = (264^\circ, 48^\circ)$, is aligned with the polar direction, and $\beta = 1.23 \times 10^{-3}$ is the magnitude of the temperature dipole [44]. In our notation this implies an asymmetry spectrum of the form

$$\delta C_{\ell \ell+1} = -2[(\ell+2)C_{\ell+1} - \ell C_\ell]. \quad (\text{C2})$$

Using this in our estimator gives us a constraint on β . With $\ell_{\text{max}} = 2000$ we obtain $\beta = (1.5 \pm 0.5) \times 10^{-3}$ in direction $(l, b) = (281^\circ, 57^\circ) \pm 22^\circ$, i.e., a roughly 3σ detection of aberration, consistent with the observed CMB dipole and the results of [25].

We are then able to remove this signal from the temperature data using the method outlined in Appendix B.2. Specifically we use Eqs. (B3) and (B4) with $\tilde{A} = -\beta$ and $\tilde{\delta C}_{\ell \ell+1}^{WZ}$ given by Eq. (C2). Note that the high- ℓ and oscillatory nature of Eq. (C2) means that this procedure only noticeably affects the results for the n_s gradient model.

-
- [1] H. K. Eriksen, F. K. Hansen, A. J. Banday, K. M. Gorski, and P. B. Lilje, *Astrophys. J.* **605**, 14 (2004), [Erratum: *Astrophys. J.* 609, 1198 (2004)], arXiv:[astro-ph/0307507](#) [astro-ph].
- [2] D. Hanson and A. Lewis, *Phys. Rev. D* **80**, 063004 (2009), arXiv:[0908.0963](#) [astro-ph.CO].
- [3] C. L. Bennett et al., *Astrophys. J. Suppl.* **192**, 17 (2011), arXiv:[1001.4758](#) [astro-ph.CO].
- [4] Planck Collaboration, *Astron. Astrophys.* **571**, A23 (2014), arXiv:[1303.5083](#) [astro-ph.CO].
- [5] Planck Collaboration, *Astron. Astrophys.* **594**, A16 (2016), arXiv:[1506.07135](#) [astro-ph.CO].
- [6] D. Scott, D. Contreras, A. Narimani, and Y.-Z. Ma, *JCAP* **1606**, 046 (2016), arXiv:[1603.03550](#) [astro-ph.CO].
- [7] C. M. Hirata, *JCAP* **0909**, 011 (2009), arXiv:[0907.0703](#) [astro-ph.CO].
- [8] R. Fernández-Cobos, P. Vielva, D. Pietrobon, A. Balbi, E. Martínez-González, and R. B. Barreiro, *Mon. Not. Roy. Astron. Soc.* **441**, 2392 (2014), arXiv:[1312.0275](#) [astro-ph.CO].
- [9] M. Yoon, D. Huterer, C. Gibelyou, A. Kovács, and I. Szapudi, *Mon. Not. Roy. Astron. Soc.* **445**, L60 (2014), arXiv:[1406.1187](#) [astro-ph.CO].
- [10] S. Baghran, A. A. Abolhasani, H. Firouzjahi, and M. H. Namjoo, *JCAP* **1412**, 036 (2014), arXiv:[1406.7277](#) [astro-ph.CO].
- [11] J. P. Zibin and D. Contreras, *Phys. Rev. D* **95**, 063011 (2017), arXiv:[1512.02618](#) [astro-ph.CO].
- [12] F. Hassani, S. Baghran, and H. Firouzjahi, *JCAP* **1605**, 044 (2016), arXiv:[1511.05534](#) [astro-ph.CO].
- [13] M. Shiraishi, J. B. Muñoz, M. Kamionkowski, and A. Raccanelli, *Phys. Rev. D* **93**, 103506 (2016), arXiv:[1603.01206](#) [astro-ph.CO].
- [14] C. Dvorkin, H. V. Peiris, and W. Hu, *Phys. Rev. D* **77**, 063008 (2008), arXiv:[0711.2321](#) [astro-ph].
- [15] F. Paci, A. Gruppuso, F. Finelli, P. Cabella, A. de Rosa, N. Mandolesi, and P. Natoli, *Mon. Not. Roy. Astron. Soc.* **407**, 399 (2010), arXiv:[1002.4745](#).
- [16] Z. Chang and S. Wang (2013), arXiv:[1312.6575](#) [astro-ph.CO].
- [17] F. Paci, A. Gruppuso, F. Finelli, A. De Rosa, N. Mandolesi, and P. Natoli, *Mon. Not. Roy. Astron. Soc.* **434**, 3071 (2013), arXiv:[1301.5195](#).
- [18] L. Dai, D. Jeong, M. Kamionkowski, and J. Chluba, *Phys. Rev. D* **87**, 123005 (2013), arXiv:[1303.6949](#) [astro-ph.CO].
- [19] S. Ghosh, R. Kothari, P. Jain, and P. K. Rath, *JCAP* **1601**, 046 (2016), arXiv:[1507.04078](#) [astro-ph.CO].
- [20] R. Kothari, S. Ghosh, P. K. Rath, G. Kashyap, and P. Jain, *Mon. Not. Roy. Astron. Soc.* **460**, 1577 (2016), arXiv:[1503.08997](#) [astro-ph.CO].
- [21] R. Kothari (2015), arXiv:[1508.03547](#) [astro-ph.CO].
- [22] M. H. Namjoo, A. A. Abolhasani, H. Assadullahi, S. Baghran, H. Firouzjahi, and D. Wands, *JCAP* **1505**, 015 (2015), arXiv:[1411.5312](#) [astro-ph.CO].
- [23] E. F. Bunn, Q. Xue, and H. Zheng, *Phys. Rev. D* **94**, 103512 (2016), arXiv:[1608.05070](#) [astro-ph.CO].
- [24] Planck Collaboration, *Astron. Astrophys.* **594**, A12 (2016), arXiv:[1509.06348](#) [astro-ph.CO].
- [25] Planck Collaboration, *Astron. Astrophys.* **571**, A27 (2014), arXiv:[1303.5087](#) [astro-ph.CO].
- [26] S. Prunet, J.-P. Uzan, F. Bernardeau, and T. Brunier, *Phys. Rev. D* **71**, 083508 (2005), arXiv:[astro-ph/0406364](#) [astro-ph].
- [27] Planck Collaboration, *Astron. Astrophys.* **594**, A20 (2016), arXiv:[1502.02114](#) [astro-ph.CO].
- [28] BICEP2/Keck/Planck Collaboration, *Phys. Rev. Lett.* **114**, 101301 (2015), arXiv:[1502.00612](#) [astro-ph.CO].
- [29] Keck Array/BICEP2 Collaboration, *Phys. Rev. Lett.* **116**, 031302 (2016), arXiv:[1510.09217](#) [astro-ph.CO].
- [30] D. Contreras, J. Hutchinson, A. Moss, D. Scott, and J. P. Zibin (2017), in preparation.
- [31] A. Moss, D. Scott, J. P. Zibin, and R. Battye, *Phys. Rev. D* **84**, 023014 (2011), arXiv:[1011.2990](#) [astro-ph.CO].
- [32] D. Scott and A. Frolop (2014), arXiv:[1403.8145](#) [astro-ph.CO].
- [33] J. Chluba, L. Dai, D. Jeong, M. Kamionkowski, and A. Yoho, *Mon. Not. Roy. Astron. Soc.* **442**, 670 (2014), arXiv:[1404.2798](#) [astro-ph.CO].
- [34] J. P. Zibin, *Phys. Rev. D* **89**, 121301 (2014), arXiv:[1404.4866](#) [astro-ph.CO].
- [35] A. Hajian and T. Souradeep, *Astrophys. J.* **597**, L5 (2003), arXiv:[astro-ph/0308001](#) [astro-ph].
- [36] A. Hajian and T. Souradeep, *Phys. Rev. D* **74**, 123521 (2006), arXiv:[astro-ph/0607153](#) [astro-ph].
- [37] Planck Collaboration, *Astron. Astrophys.* **571**, A17 (2014), arXiv:[1303.5077](#) [astro-ph.CO].
- [38] Planck Collaboration, *Astron. Astrophys.* **594**, A15 (2016), arXiv:[1502.01591](#) [astro-ph.CO].
- [39] Planck Collaboration, *Astron. Astrophys.* **594**, A9 (2016), arXiv:[1502.05956](#) [astro-ph.CO].
- [40] P. C. Gregory, *Bayesian Logical Data Analysis for the Physical Sciences* (Cambridge University Press, 2005).
- [41] CMB-S4 Collaboration (2016), arXiv:[1610.02743](#) [astro-ph.CO].
- [42] J. Delabrouille, P. de Bernardis, F. R. Bouchet, and the CORE Collaboration, A proposal in response to the ESA call for a Medium Size space mission for launch in 2029-2030 (2016).
- [43] A. Challinor and F. van Leeuwen, *Phys. Rev. D* **65**, 103001 (2002), arXiv:[astro-ph/0112457](#) [astro-ph].
- [44] Planck Collaboration, *Astron. Astrophys.* **594**, A8 (2016), arXiv:[1502.01587](#) [astro-ph.CO].
- [45] One particularly motivated model of this form would be a modulated integrated Sachs-Wolfe component, which will be examined in [30].
- [46] A similar result for tensors was alluded to in [32].